Journal of Nuclear Materials 517 (2019) 9–16

Contents lists available at ScienceDirect

Journal of Nuclear Materials

journal homepage: www.elsevier.com/locate/jnucmat

Channeling analysis in studying ion irradiation damage in materials containing various types of defects☆

Ke Jin [a], Gihan Velisa [a], Haizhou Xue [b], Taini Yang [c], Hongbin Bei [a], William J. Weber [b, a], Lumin Wang [c], Yanwen Zhang [a, b, *]

[a] Materials Science & Technology Division, Oak Ridge National Laboratory, Oak Ridge, TN, 37831, USA
[b] Department of Materials Science and Engineering, University of Tennessee, Knoxville, TN, 37996, USA
[c] Department of Nuclear Engineering and Radiological Sciences, University of Michigan, Ann Arbor, MI, 48109, USA

HIGHLIGHTS

- Dechanneling analysis is valid for materials containing various types of defects.
- Pure dechanneling assumption in irradiated metals is oversimplified.
- Lack of damage peak does not mean lack of direct-backscattering sources.
- Information on defect types can be obtained from dechanneling analysis.

ARTICLE INFO

Article history:
Received 26 February 2018
Received in revised form
7 December 2018
Accepted 21 January 2019
Available online 22 January 2019

Keywords:
RBS
Ion channeling
Ion irradiation
Dechanneling
Damage accumulation

ABSTRACT

Ion channeling is a powerful quantitative technique for studying ion-irradiation induced defect evolution in single crystalline materials. An iterative procedure to determine dechanneling yields has been developed for decades, serving as a major method for analyzing experimental channeling data. The applicability of such procedure is, however, generally limited to the crystalline damage with only point defects and local amorphous domains. For the other cases, such as irradiated metals, the assumption of direct-backscattering free has usually been made. In the present study, Ni, TiAl, MgO, and $SrTiO_3$ single crystals are selected as four model materials, representing metals, intermetallic alloys, and ceramic compounds with different defect evolution processes under irradiation, to investigate the fidelity of applying dechanneling analysis on various types of defects. The pure dechanneling assumption is shown oversimplified in Ni irradiated with low fluence self-ions and may result in error on the derived damage profile. Moreover, the iterative procedure of dechanneling analysis is shown valid for more general situations than the randomly distributed atoms, including those not exhibiting a peak in channeling spectra. The disappearance of damage peak in channeling spectra is attributed to the combined effects of small (but non-zero) scattering factor, long-range damage effects, and non-ignorable damage level in pristine crystals. Furthermore, the ratio of direct backscattering to dechanneling areas provides information on defect configurations in the materials containing a well-defined damage peak in channeling spectra. The contribution from dechanneling sources increases from $SrTiO_3$, TiAl, to MgO, according to the derived scattering and dechanneling factors.

1. Introduction

Characterizing and understanding ion-irradiation induced damage accumulation in materials are important in material science, semiconductor engineering, and nuclear energy applications [1–3]. Among various types of characterization techniques, Rutherford backscattering spectrometry in its channeling mode (RBS/C, or ion channeling) has been broadly used as a non-destructive,

☆ This manuscript has been authored by UT-Battelle, LLC under Contract No. DE-AC05-00OR22725 with the U.S. Department of Energy. The United States Government retains and the publisher, by accepting the article for publication, acknowledges that the United States Government retains a non-exclusive, paid-up, irrevocable, world-wide license to publish or reproduce the published form of this manuscript, or allow others to do so, for United States Government purposes. The Department of Energy will provide public access to these results of federally sponsored research in accordance with the DOE Public Access Plan.

* Corresponding author. Materials Science & Technology Division, Oak Ridge National Laboratory, Oak Ridge, TN, 37831, USA.
E-mail address: zhangy1@ornl.gov (Y. Zhang).

https://doi.org/10.1016/j.jnucmat.2019.01.033
0022-3115/

depth-resolved, mass-resolved, and quantitative technique for detecting defects and disorders in single-crystalline materials [4,5]. The advantage on its application is further highlighted as its detection depth, usually sub-micron, is well comparable with typical ion-irradiation induced damage range.

In spite of these significant merits, direct quantitative analysis of ion channeling spectra is in general not straightforward resulting from the complex interactions between incident probe ions and the lattice imperfections: 1) some channeled ions can be directly backscattered by the displaced atoms, and 2) some channeled ions can be slightly deflected into a non-channeled direction, behaving as a beam in random directions (so-called dechanneling) [4]. For the analysis purpose, normalized RBS yield of a damaged sample, χ_D, can be treated as composed of two fractions: 1) dechanneling yield, χ_R, resulting from the dechanneled (random) fraction of the beam, and 2) yield from the channeled beam directly backscattered by the defects. This mechanism can be mathematically expressed as follows,

$$\chi_D(z) = \chi_R(z) + [1 - \chi_R(z)]fN_D(z) \tag{1}$$

$$\chi_R(z) = \chi_V(z) + \left[1 - \chi_V(z)\right]\left[1 - \exp\left(-\int_0^z \sigma_D N_D(z')dz'\right)\right] \tag{2}$$

where χ_V is the pristine level, N_D is the relative defect density, and z is the thickness of the damage layer from the sample surface. The defect scattering factor, f, and dechanneling factor, σ_D, depend on the parameters of material lattice, defects (configuration, size, etc.), and probe beam (energy, incident direction, etc). These two factors are usually unknown for regular experiments and need pre-assumptions input.

The above two equations have been considered difficult to be deconvoluted, except in two extreme conditions. The first case is for dislocation lines, in which $f = 0$ (pure dechanneling), and the dislocation density can be directly extracted by

$$N_D(z) = \frac{1}{\sigma_D}\frac{d}{dz}\left\{Ln\left[\frac{1 - \chi_V(z)}{1 - \chi_D(z)}\right]\right\} \tag{3}$$

The second case is for randomly displaced atoms, in which $f = 1$, and Eq. (1) is then simplified into

$$\chi_D(z) = \chi_R(z) + [1 - \chi_R(z)]N_D(z) \tag{4}$$

In this case, Eqs. (4) and (2) together can then be solved using a well-developed *Iteration Procedure* (*IP*), in which σ_D is a tuning parameter and determined when the χ_R curve overlaps with χ_D at the depth after which the defect density is assumed zero. The detailed numerical process has been provided in several literature, such as Ref. [6,7], and will not be repeated here. The *IP* mentioned in the following text is referred to this established process.

When encountering more general cases ($0 < f < 1$), e.g. for materials containing small dislocation loops, stacking fault tetrahedra (SFT), or mixed defects, a number of previous studies have made assumptions that ignore the defect complexity (e.g., assuming pure dechanneling in ion-irradiated metals [4,8–10]). In the recent years, simulations (e.g., Monte Carlo) have been developed to simulate the channeling spectra containing multiple and complex types of defects [11–14]. However, in addition to high computing cost, such simulations usually need pre-input of detailed defect information, such as defect types and configurations, for each specific case, which are either from assumptions or microscopic observations in advance.

In the present study, the fidelity of applying *IP* on various types of defects is investigated. Ni is selected to examine the applicability of pure dechanneling assumption in those irradiated metals that contain primarily dislocation (loops) and SFT, rather than random displaced atoms or amorphous regions. Moreover, the validity of the *IP* on the materials containing extended defects is demonstrated, and the origins of the disappearance of damage peaks in channeling spectra are discussed. Furthermore, dechanneling analyses are performed in ion irradiated MgO, $SrTiO_3$, and TiAl, as representatives for radiation resistant ceramics, radiation sensitive ceramics, and radiation sensitive alloys (intermetallics), respectively. In addition to the conventional damage accumulation analysis, different defect scattering and dechanneling factors are observed in these materials, revealing information on different types of defect configurations.

2. Experimental

Four model single crystalline materials, pure Ni, $SrTiO_3$, MgO, and TiAl were selected to study the ion irradiation induced damage using the ion channeling technique. They were irradiated with 1.5 MeV Ni, 900 keV Au, 1 MeV Au, and 900 keV Ti ions, respectively, using the tandem accelerator at the Ion Beam Materials Laboratory located at the University of Tennessee [15]. All irradiations were performed at room temperature, in directions a few degrees off surface normal to avoid channeling irradiations. The displacement profiles were simulated using the Stopping and Range of Ions (SRIM) code. For a convenient comparison with the literature regarding these materials, the full-cascade mode was used for the two ceramics, while the Kinchin-Pease (K–P) mode was used for Ni and TiAl. The threshold displacement energies (E_d) were assumed as follows: 40 eV for Ni [16], 55 eV for both Mg and O atoms in MgO [13,17], 80, 70, and 45 eV for Sr, Ti, and O atoms in $SrTiO_3$, respectively [15], and 28 and 34 eV for Ti and Al atoms in TiAl, respectively [18]. Under such assumptions, the peak irradiation dose was 0.13 displacements per atom (dpa) for Ni. The peak dose ranges in $SrTiO_3$, MgO, and TiAl were 0.13–0.32, 0.17–0.69, and 0.29–1.2 dpa, respectively. The peak dose rates for all the four materials were within the range of $0.6–2 \times 10^{-3}$ dpa/s.

The ion channeling analyses were performed using 3.5 MeV He ions as the probe beam for analyzing Ni, $SrTiO_3$, and TiAl, while 3 MeV He ions were used for MgO to avoid non-Rutherford cross-section for Mg signal. A silicon detector was located at the scattering angle of 155° from the incoming beam [15]. Furthermore, cross-sectional transmission electron microscopy (TEM) was utilized to examine the depth dependence of damage produced in a Ni sample irradiated with 1.33 MeV Mn ions at room temperature to the peak dose of 0.05 dpa.

3. Results and discussions

3.1. Examination of the pure dechanneling assumption in irradiated metals

While the point defect assumption ($f = 1$) has been mostly used in the cases of ceramics, the pure dechanneling assumption ($f = 0$) has been commonly made when studying irradiated metals from the early years till present. A number of these studies have directly used Eq. (3); [8,9,16] the others have used a further simplified model that, since the defect density is approximately proportional to the slope of χ_D, the end of damage should appear at the knee point after which the slope decreases and becomes closer to the pristine level [10,19–22]. This assumption for irradiated metals has been made considering the fact that, in common metals irradiated with ions at the energy range of hundreds of keV to a few MeV, both point defects and amorphous region are hardly formed at room temperatures and above, extended defects grow into dislocation loops with increasing fluence, and dislocation networks may form after high fluence irradiations [2]. The pure dechanneling assumption in irradiated metals has also been compared with either the simulated depth distribution of displacements (e.g. by

SRIM) or the measured implanted ion profiles [4,16], and the major trend of damage accumulation has been confirmed or in agreement to a certain extent.

Nonetheless, small dislocation loops and SFT with sizes less than a few nanometers (e.g. the black-dot defects in TEM observations) are also formed in irradiated metals, and are dominant when the irradiation is in the low and medium dose regime [23–25]. Even for high dose irradiated pure metals (e.g. Cu), ion channeling studies have observed the defect nature of interstitial atoms based on an energy dependent study [20], although the damage range was also determined by the knee point in that study. The scattering of incident ions by these small defect clusters are different from that by dislocation lines, and the direct backscattering may no longer be negligible [4]. In these cases, the use of pure dechanneling assumption becomes questionable.

One example is for pure Ni irradiated with 1.5 MeV Ni ions at room temperature. Fig. 1a shows the channeling spectrum at the irradiation fluence of 1×10^{14} cm^{-2}, corresponding to the dose of ~0.3 dpa at the displacement peak at ~400 nm. The knee point is marked by the cross of the line fittings, which should indicate the end of damage if assuming the pure dechanneling assumption analysis is valid. The dechanneling parameter profile derived from Eq. (3) is shown in Fig. 1b as the solid red line, which should be proportional to the defect density profile under the pure dechanneling assumption. The end of damage in this curve is close to the knee point position in Fig. 1a, as expected. The SRIM predicted displacement profile is also shown for comparison.

Both the derived damage peak position and the total damage range from the pure dechanneling assumption ($f = 0$) are ~30% shallower than those predicted by SRIM. In fact, it is well known that the actual damage range in FCC metal single crystals is usually greater than the simulated displacement range at high irradiation doses, so-called the long-range effect, due to the combined origins such as defect migrations and channeling irradiations [22,26,27]. Fig. 1c and d shows a representative case of low dose irradiations, i.e. pure Ni irradiated with 1.33 MeV Mn ions (similar to the irradiation condition for 1.5 MeV Ni ions) to a low fluence of 4×10^{13} cm^{-2}, corresponding to the peak dose of ~0.05 dpa. As shown in Fig. 1d, the peak position of the damage profile obtained from cross-sectional TEM bright field imaging (inset of Fig. 1c), similar to the damage profile extracted based on the *IP*, is slightly deeper than the SRIM prediction, and a damage tail is observed. Consequently, the shallow damage range derived based on the pure dechanneling assumption is unrealistic and thus $f \neq 0$, consistent to the fact that under this irradiation condition small defect clusters (dislocation loops and SFT) are the dominant defect types (see Fig. 1c).

When following the *IP* based on Eqs. (4) and (2), the dechanneling fraction of the channeling yield is shown as the green dash curve in Fig. 1a, and the direct backscattering fraction is then the shade area. The derived damage profile is shown in Fig. 1b and d as the dash-dot line, which agrees much better to the SRIM prediction, supported by our TEM observations. The damage tail beyond the SRIM predicted displacement range is also observed by TEM and detected from RBS/C.

Note that the *IP* was conventionally used only under the assumption of point defects ($f = 1$) unless a known f value is assigned, which is clearly not the case in pure Ni ($0 < f < 1$). Thus, the questions become: is it reasonable to use this method in materials containing extended defects or even mixed defects, and, if yes, what information can be extracted and what are the limitations.

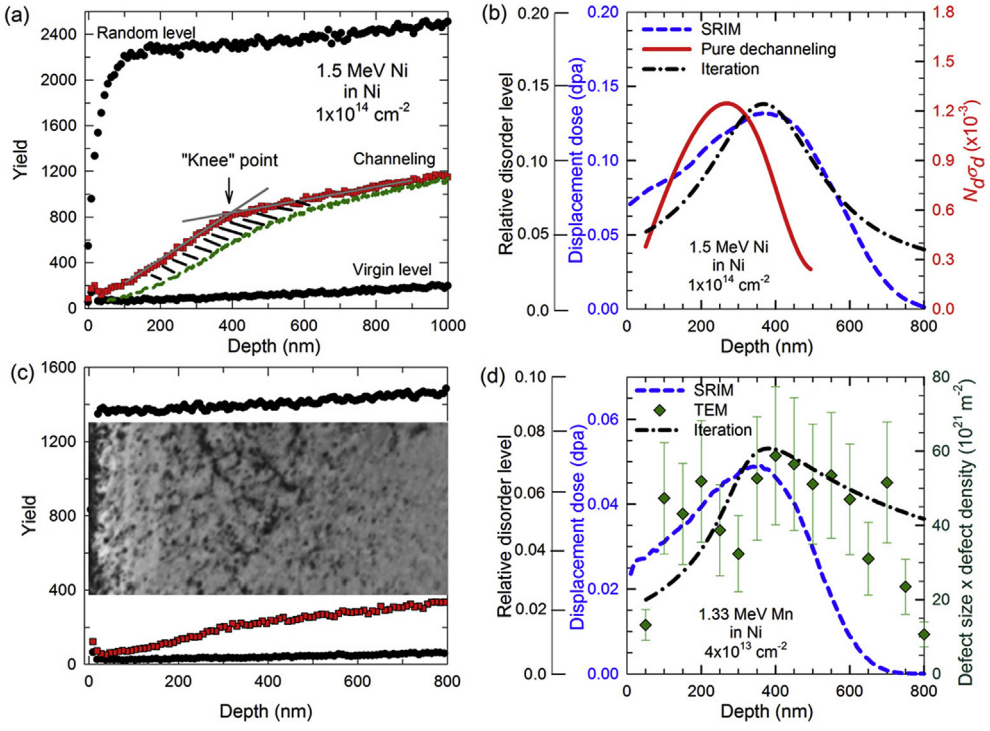

Fig. 1. (a) RBS/C spectra for Ni irradiated with 1.5 MeV self-ions to a fluence of 1×10^{14} cm^{-2}. The green dash line is the dechanneling fraction derived based on the *IP*. (b) Displacement profile from SRIM simulation (blue dash line), and the damage profile extracted based on pure dechanneling assumption (solid line) and the *IP* (dash-dot line). (c) RBS/C spectra and the corresponding cross-sectional TEM bright field image of Ni irradiated with 1.33 MeV Mn ions to 4×10^{13} cm^{-2}. The depth scale in x-axis also applies to the TEM image. (d) Extracted depth profile of (defect size) × (defect density) from TEM (diamond), the damage profile extracted based on the *IP* (dash-dot line), and the displacement profile from SRIM prediction (dash line) from the data/image of (c). (For interpretation of the references to colour in this figure legend, the reader is referred to the Web version of this article.)

3.2. Generalized application of IP for defects with $0 < f < 1$

3.2.1. For materials containing small extended defects

Small extended defects, such as dislocation loops of a few nanometers, cause local strain and non-ignorable contribution of direct backscattering, resulting in the scattering factor f between 0 and 1. If we define scaled defect density and dechanneling factor

$$N_D^{'}(z) = fN_D(z) \tag{5}$$

and

$$\sigma_D^{'} = \sigma_D / f \tag{6}$$

Eqs. (1) and (2) become

$$\chi_D(z) = \chi_R(z) + [1 - \chi_R(z)]N_D^{'}(z) \tag{7}$$

and

$$\chi_R(z) = \chi_V(z) + \left[1 - \chi_V(z)\right]\left[1 - \exp(-\int_0^z \sigma_D^{'} N_D^{'}(z^{'})dz^{'})\right] \tag{8}$$

which have the same format of Eqs. (4) and (2), and can thus be mathematically solved equivalent as the case of point defects, except that here only σ'_D and thus $N'_D(z)$ can be determined. The actual defect density cannot be directly solved since f is unknown, however, the purposes of understanding damage accumulation process and making comparison between different materials can be reasonably achieved from the $N'_D(z)$ profiles. With decreasing f, the dechanneling profile (the green dash line in Fig. 1a) keeps approaching the channeling spectra. When f comes to zero, σ'_D becomes infinite large and this method is no longer valid. In the example of irradiated Ni in Sec. 3.1, the defect scattering factor is non-zero due to the existence of small defect clusters, and thus the direct use of *IP* is valid, and the derived results are the profile of fN_d.

3.2.2. For materials containing both point defects and dislocations

Now consider a more complex but more realistic case, a sample containing two types of defects, with (f_1, σ_{D1}) and (f_2, σ_{D2}). For simplicity, defect type-1 is assumed to be a pure dechanneling source (e.g. dislocation lines), that is $f_1 = 0$, and defect type-2 is arbitrary (e.g., randomly displaced atoms, extended defect clusters, and amorphous domains where $0 \le f \le 1$). Then Eqs. (1) and (2) can be written as

$$\chi_D(z) = \chi_R(z) + [1 - \chi_R(z)]f_2 N_{D2}(z) \tag{9}$$

$$\chi_R(z) = \chi_V(z) + \left[1 - \chi_V(z)\right]\left[1 - \exp(-\int_0^z (\sigma_{D1}N_{D1}(z') + \sigma_{D2}N_{D2}(z'))dz')\right] \tag{10}$$

Assuming the different types of defects have the same depth distribution, and

$$N_{D1}(z)/N_{D2}(z) = \text{constant C} \tag{11}$$

the scaled defect density and dechanneling factor can then be redefined as

$$N_D^* = f_2 N_{D2}(z) \tag{12}$$

and

$$\sigma_D^* = (\sigma_{D1}C + \sigma_{D2})/f_2 \tag{13}$$

which makes Eqs. (9) and (10) become

$$\chi_D(z) = \chi_R(z) + [1 - \chi_R(z)]N_D^*(z) \tag{14}$$

and

$$\chi_R(z) = \chi_V(z) + \left[1 - \chi_V(z)\right]\left[1 - \exp(-\int_0^z \sigma_D^* N_D^*(z')dz')\right] \tag{15}$$

Similar to Eqs. (7) and (8), Eqs. (14) and (15) also have the same format as Eqs. (4) and (2), suggesting that the *IP* is still valid in this case, with the notation that the fitting parameter becomes σ^*_D, and the derived damage profile is the profile of $f_2N_{D2}(z)$, and the density of the pure dechanneling source is CN^*_D/f_2.

A special case can now be considered for a combination of pure dechanneling source and point defect source, i.e. $f_1 = 0$ and $f_2 = 1$. In this case, the derived defect density profile from the *IP* is equal to that of the point defect density distribution. The density of dislocation lines is only determined by the factor C, which is unable to be derived from the present dechanneling analysis. However, since the dechanneling factor of dechanneling source is at least a few orders larger than that for point defects, σ^*_D is then equal to $\sigma_{D1}C$. If the theoretical value of dechanneling factor of the dislocation lines can be calculated, the constant C can be derived from the comparison of the fitting value, σ^*_D, and the theoretical value, σ_{D1}.

Consequently, in principle, the use of *IP* for dechanneling analyses does not require the pre-assumption of point defects for comparison and the semi-quantitative analysis on the damage accumulation. Note that the situation can be more complicated in actual irradiated samples, since the dechanneling and scattering factors of defects, e.g. dislocation loops, depend not only on their type and size, but also on the relative direction between the incident beam and defect orientation. Thus, the fit values from dechanneling analysis should be treated as a value of effective average. In fact, even for irradiated ceramics, in which the defects are usually treated as non-extended, the defects inside are not always fully uncorrelated point defects, and the derived $N_D(z)$ has been shown not necessarily the actual defect density or absolute disorder level [13,14,28], depending on the defect configurations.

3.2.3. Indications from the disappearance of damage peak in channeling spectra

In most cases where *IP* has been conventionally applied, a peak in the channeling spectra is observed (see examples in Refs. [4,6,7] and those in the following Section 3.3). However, the lack of such damage peak in channeling spectra has been seen in irradiated metals, as shown in Fig. 1a. In other words, the channeling spectra for most irradiated materials has a downhill region where backscattering yield decreases, while those for many metals keep increasing across the entire depth beyond the end of damage. This difference has been considered as an indication of pure dechanneling, but in Section 3.1 such assumption has been proved to be wrong or unnecessary, and the *IP* has been demonstrated also valid.

To interpret this qualitative discrepancy without considering details of defect distribution, we examine the derivative of channeling spectra, $d\chi_D(z)/dz$, just before the end of defective region, z_m, where by definition the defect density $N_D(z_m) = 0$ and density slope $N'_D(z_m) < 0$. Moreover, at this depth, $\chi_R = \chi_D$, according to the nature of *IP*. Note that, this analysis only depends on the existence of z_m, but not consider where it is located.

If we define $I(z)$ as the integrated defect density, i.e. $dI(z)/$

$dz = N_D(z)$, and assume low defect density, Eqs. (1) and (2) can be re-written into

$$\chi_D(z) = \chi_V(z) + fN_D(z)[1 - \chi_V(z)] + \sigma_D I(z)[1 - \chi_V(z)][1 - fN_D(z)] \quad (16)$$

Note again the features of z_m, we have

$$\sigma_D \cdot I(z_m) = [\chi_D(z_m) - \chi_V(z_m)]/[1 - \chi_V(z_m)] \quad (17)$$

and

$$\frac{d\chi_D(z)}{dz}_{z=z_m} = \frac{1 - \chi_D(z_m)}{1 - \chi_V(z_m)} \left\{ f \cdot N_D'(z_m) \cdot [1 - \chi_V(z_m)] + \chi_V'(z_m) \right\} \quad (18)$$

Eq. (18) can be further simplified, if assuming ignorable virgin level $\chi_V(z) = 0$, into

$$\chi_D'(z_m) = [1 - \chi_D(z_m)] \cdot f \cdot N_D'(z_m) \quad (19)$$

Under this assumption of ignorable virgin level, the slope of channeling yield must be negative when $f > 0$ and the material is not fully amorphous, since $\chi_D(z) \leq 1$ (equity is reached only when fully amorphous), and $N'_D(z_m) < 0$. In other words, there exists at least one local maximum in the channeling spectrum before the end of damage, which is contradictory to the experimental findings such as in Fig. 1a.

When considering Eq. (18) with non-zero virgin levels, the sign of the slope of channeling spectrum depends on two competing terms: a negative term $f\,N'_D(z_m)\,[1\text{-}\chi_V(z_m)]$, and a positive term $\chi'_V(z_m)$. Note that the positive term is very small in high-quality crystalline samples, and thus the overall slope is usually negative (containing a region of declining yield between the peak and the end of damage) in most common non-metal situations. However, in irradiated metals such as Ni (Fig. 1a), two reasons might cause an overall positive slope: 1) the small scattering factor value, f, while non-zero, can greatly reduce the negative term, and 2) the irradiation induced defect can reach much deeper depth than the end of displacement profile predicted by SRIM [22], causing a gentle decrease of defect density, meaning a small $N'(z_m)$. In such cases, the negative term may be smaller than the positive one, causing the overall positive slope.

Two additional supportive evidences can be seen from the simulation studies [12]. First, the drop of channeling yield is less sharp at the set point of the end of damage for materials containing extended defects, compared with those containing point defects. Second, when simulating experimental spectra, the fitted defect density does not decrease to zero in the simulation depth regime. This second phenomenon can also be observed when applying the *IP*, see Fig. 1b. Although Eq. (18) applies only at the depth of damage end, it demonstrates in principle the origin of the lack of damage peak shown in the channeling spectra. It needs to be emphasized that the lack of appearance of damage peak does not necessarily indicate lack of direct backscattering centers.

3.3. Channeling analysis when damage peaks appear

The analysis of ion channeling spectra containing a damage peak, in either ceramics or alloys, has been well-developed in the past decades. Here three examples are shown in Fig. 2a–c for the relative channeling yield, χ_D, at various irradiation doses for 900 keV Au ion irradiated $SrTiO_3$, 1 MeV Au ion irradiated MgO, and 900 keV Ti ion irradiated TiAl, respectively. Only the yields from Sr, Mg, and Ti signals (the heaviest elements in the compounds) are shown for comparison due to their less experimental uncertainty. Damage accumulation process can be derived based on Eqs. (4) and (2), or, equivalently Eqs. (7) and (8), using the *IP*, no matter whether we treat them as in point-defect limit or not. Fig. 2d shows the derived relative disorder as a function of irradiation dose at the SRIM-predicted damage peak region.

The knowledge of defect scattering factor, f, is necessary to clarify the meaning of the derived relative disorder level, see Eqs. (5) and (12). However, obtaining the structural information of the defects can hardly be done by directly using the *IP* when analyzing channeling spectra, and usually demands computational simulation codes such as DICADA [29], McChasy [28], and RBSADEC [12] to fit the experimental spectra. Here we demonstrate that, other than disorder level, the value of f can also be semi-quantitatively estimated from the channeling and dechanneling profiles. Fig. 3a shows a typical dechanneling analysis for a well-defined damage peak, taken $SrTiO_3$ irradiated with 900 keV Au to 5.2×10^{13} cm^{-2} (~0.2 peak dpa) as an example. The green squares are the relative channeling yield, χ_D, from the measurements, the black dots at bottom are the relative channeling yield from the pristine sample, χ_V, and the blue curve is the derived χ_R from the *IP*. Two areas, $Area_D$ and $Area_R$, between the curves represent the signal from direct backscattering and from dechanneled ions, respectively.

If assuming low defect density and ignorable virgin level for simplicity, the ratio of the two areas (from surface to the end of damage zone), *AR*, can then be written as

$$AR = \frac{Area_D}{Area_R} = \frac{\int_0^{z_m} fN_D(z)[1 - \sigma_D I(z)]dz}{\int_0^{z_m} \sigma_D I(z)dz} \quad (20)$$

Although the general apparent expression of Eq. (20) is not available due to the unknown defect density distribution, two special cases can be derived analytically. First, if assuming uniform defect density, i.e. $N_D(z) = N_u$, the area ratio can be written as

$$AR = fN_u[2/\chi_D(z_m) - 1] \quad (21)$$

Another more complicated but possibly more realistic situation is that the defect density increases from 0 linearly to the maximum disorder, N_m, at half of maximum damage range, and then linearly decreases to 0. For defect concentration profiles in such shape, the area ratio can be approximately reduced to

$$AR = fN_m[2/\chi_D(z_m) - 1]/2 \quad (22)$$

Note that *AR* and $\chi_D(z_m)$ can both be obtained from the dechanneling analysis process. The values $2AR/[2/\chi_D(z_m) - 1]$ for the three tested materials are plotted in Fig. 3b as a function of measured peak relative disorder based on the *IP*, N_m, to the first order approximation. It can be seen that the data points of $SrTiO_3$ follow very well to the solid line, suggesting $f = 1$, which can be expected since the defects created at room temperature from Au ion irradiation are mainly random point defects or local amorphous domain [30]. The data for MgO are deviated from the unit slope, down to about 0.83, suggesting that a more organized defect structure is formed. This is consistent with the previous results that small dislocation loops are formed and aggregated into dislocation networks with increasing irradiation dose [13]. The data of TiAl is somewhat more scattered, but essentially the derived scattering factor for all the three materials are large and within 20% difference, which is very different from those without showing damage peaks (e.g. Ni). Here we want to emphasize that the absolute value here may not be accurate, since the model for Eq. (22) is apparently oversimplified. However, it provides a qualitative comparison and information on radiation response that the higher f value the higher

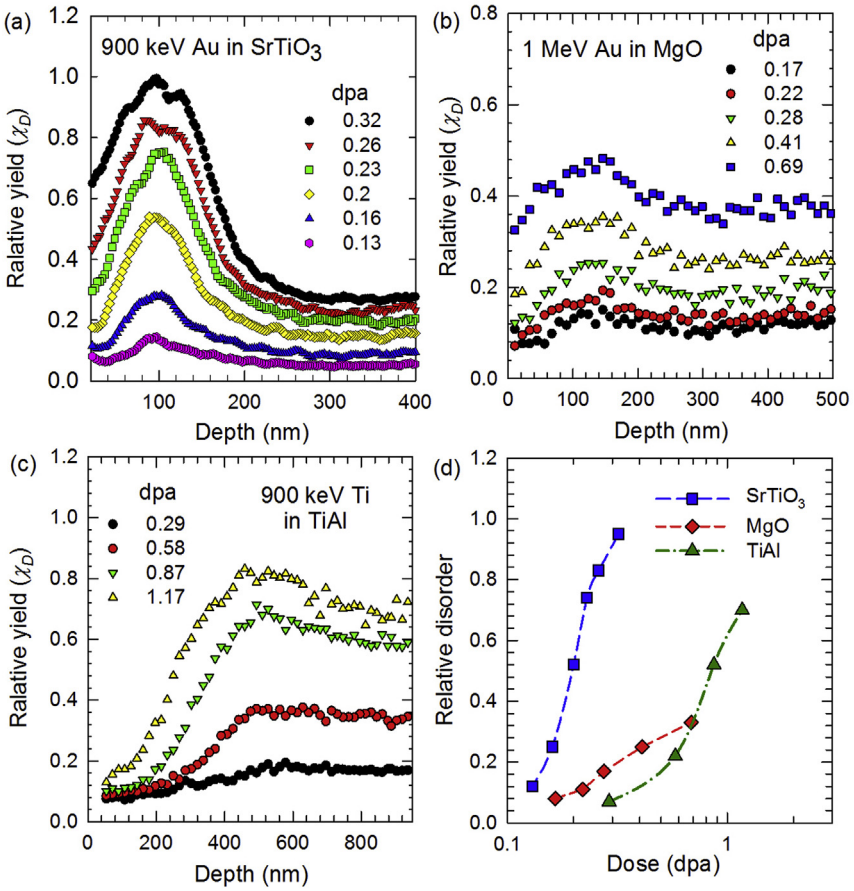

Fig. 2. Relative yield of the channeling spectra of (a) $SrTiO_3$ irradiated with 900 keV Au ions, (b) MgO irradiated with 1 MeV Au ions, and (c) TiAl irradiated with 900 keV Ti ions. (d) Relative disorder taken from the damage peak as a function of peak irradiation dose for the three materials derived using the typical *IP* approach.

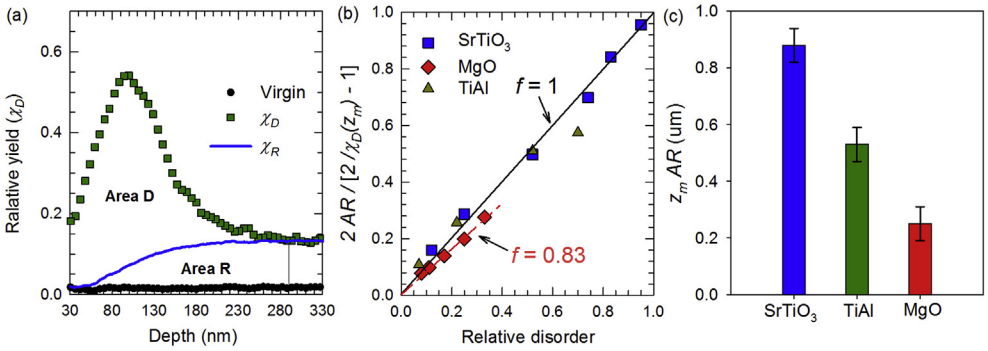

Fig. 3. (a) Dechanneling analysis profiles for $SrTiO_3$ irradiated with 900 keV Au to ~0.2 peak dpa. Area D is referred to the region between the channeling profile χ_D and the dechanneling profile χ_R. Area R is referred to the region between χ_R and the pristine level. (b) Normalized area ratio as a function of relative disorder level. (c) Product of damage range and area ratio for different compounds, extrapolated to zero disorder.

ratio of direct backscattering-dominant centers (e.g. randomly displaced atoms) vs. the dechanneling-dominant centers (e.g. atoms in extended defects).

If extrapolating the disorder level (determined based on the *IP*) down to 0, the product of damage range and *AR* is then proportional to the ratio of scattering factor, *f*, and dechanneling factor, σ_D.

$$z_m\, AR \sim f \,/\, \sigma_{\mathrm{D}} \tag{23}$$

The values of such normalized area ratios are 0.88, 0.53, and 0.25, for $SrTiO_3$, TiAl, and MgO, respectively, as shown in Fig. 3c. Considering the similar scattering factor of these three materials (see Fig. 3b), this relatively large difference among the three materials is mainly attributed to their different dechanneling factor: $SrTiO_3$ has the lowest dechanneling factor, while the MgO has the greatest value. This result also agrees with their different defect evolution processes under irradiation [6,13,30].

It needs to be further noted that this analysis is more challenging for the case of materials without exhibiting a clear damage peak due to the following two reasons: 1) the direct scattering fraction is usually too small for accurate quantification (see Figs. 1a) and 2) without a clear peak shown in the channeling spectra, the

determination of the end of damage may rely on additional inputs and may cause additional uncertainty, see discussions in Section 3.2.3. It is worth noting that electronic stopping powers for an energetic He beam used for RBS measurement can be significantly reduced in a perfectly aligned crystal that is free from any defects, which may lead to underestimation of the energy-to-depth conversion. Given the limited available database of stopping powers in pristine and damage crystals, all the energy-depth conversion in the present RBS analyses relies on the electronic stopping power of He ions along a random direction. Further investigations are desired to address these issues and to provide improved analysis procedure, and simulation works may be necessary to provide the absolute quantification of defect density.

4. Conclusions

In summary, the present work has performed channeling analyses on four irradiated model materials, pure Ni, $SrTiO_3$, MgO, and TiAl to examine the assumptions and fidelity of the analysis methods in studying ion irradiation induced damage accumulation. It has been demonstrated that:

(1) The assumption of pure dechanneling source in irradiated metal may be oversimplified, especially in the low dose regime where small (less than a few nanometer) defect clusters are dominant, and may result in error on determining the damage profile.
(2) The *IP* approach, initially developed for analyzing the ceramics containing only point defects or with pre-assigned scattering factors, can also be applied to more general cases with unknown defect scattering factor *f* between 0 and 1, and multiple types of defects. The meaning of extracted disorder profile in such cases has been clarified as the product of scattering factor and the density of scattering centers.
(3) The vanish of damage peak in the channeling spectra for irradiated metals, such as pure Ni, has been shown not necessarily an evidence of pure dechanneling assumption, but attributed to the combined effects of the small (but non-zero) scattering factor, the small negative defect concentration gradient close to the end of damage range due to the long-range damage effects, and the non-ignorable virgin level.
(4) Besides relative disorder level, the normalized area ratio between direct backscattering fraction and the dechanneling fraction contains information on the defect configuration, based on the derived scattering and dechanneling factors. For example, point defects or local amorphous domains are dominant in $SrTiO_3$, resulting in high scattering and low dechanneling factors. Extended or ordered defects (e.g., dislocation loops or dislocation network) are formed in MgO at a relatively low disorder level, and result in reduced scattering and enhanced dechanneling factors. The analyses of TiAl suggest that the extended defects have less dechanneling contribution, as compared with MgO.

By expanding the scope of using channeling analysis in different kinds of irradiated materials containing various types of defects, the present study may contribute to accelerating the understanding of irradiation-induced defect evolution and advance the development of nuclear materials.

Acknowledgements

The work in Ni and TiAl was supported as part of the Energy Dissipation to Defect Evolution (EDDE), an Energy Frontier Research Center funded by the U.S. Department of Energy, Office of Science, Basic Energy Sciences under contract number DE-AC05-00OR22725. The work in ceramics ($SrTiO_3$ and MgO) was supported by the U.S. Department of Energy, Office of Science, Basic Energy Sciences, Materials Sciences and Engineering Division. H.X. acknowledges support from the University of Tennessee Governor's Chair program.

Appendix A. Supplementary data

Supplementary data to this article can be found online at https://doi.org/10.1016/j.jnucmat.2019.01.033.

5. Conflicts of interest

The authors declare no competing interests.

References

[1] S.J. Zinkle, G.S. Was, Materials challenges in nuclear energy, Acta Mater. 61 (2013) 735–758.
[2] G.S. Was, Fundamentals of Radiation Materials Science: Metals and Alloys, Springer, Berlin, Heidelberg, New York, 2007.
[3] W.J. Weber, R.C. Ewing, C.R.A. Catlow, T.D. de la Rubia, L.W. Hobbs, C. Kinoshita, H. Matzke, A.T. Motta, M. Nastasi, E.K.H. Salje, E.R. Vance, S.J. Zinkle, Radiation effects in crystalline ceramics for the immobilization of high-level nuclear waste and plutonium, J. Mater. Res. 13 (1998) 1434–1484.
[4] L.C. Feldman, J.W. Mayer, S.T. Picraux, Materials Analysis by Ion Channeling, Academic Press, 1982.
[5] W.-K. Chu, J.W. Mayer, M.A. Nicolet, Backscattering Spectrometry, Academic Press, Inc., 1978.
[6] Y. Zhang, J. Lian, Z. Zhu, W.D. Bennett, L.V. Saraf, J.L. Rausch, C.A. Hendricks, R.C. Ewing, W.J. Weber, Response of strontium titanate to ion and electron irradiation, J. Nucl. Mater. 389 (2009) 303–310.
[7] L. Shao, M. Nastasi, Methods for the accurate analysis of channeling Rutherford backscattering spectrometry, Appl. Phys. Lett. 87 (2005), 064103.
[8] M. Vos, D.O. Boerma, Lattice damage in single crystals of Cu after self-implantation studied by channeling, Nucl. Instrum. Methods Phys. Res. B 15 (1986) 337–340.
[9] S.B. Dabagov, G.D. Tolstolutskaya, I.E. Kopanetz, I.M. Neklyudov, Radiation damage, range distribution, and site location measurements by channeling technique for Ar, Kr, Xe in Ni after implantation and annealing, SPIE Proc. 6634 (2007) 66340W–66341W.
[10] Y. Fujino, Y. Igarashi, S. Nagata, Ion-beam irradiation of Cu and a Cu-Ni alloy single-crystal specimens: proposed atom movement mechanism, Phys. Rev. B 63 (2001) 100101 (R).
[11] L. Nowicki, A. Turos, R. Ratajczak, A. Stonert, F. Garrido, Modern analysis of ion channeling data by Monte Carlo simulations, Nucl. Instrum. Methods Phys. Res. B 240 (2005) 277–282.
[12] S. Zhang, K. Nordlund, F. Djurabekova, Y. Zhang, G. Velisa, T.S. Wang, Simulation of Rutherford backscattering spectrometry from arbitrary atom structures, Phys. Rev. E 94 (2016), 043319.
[13] S. Moll, Y. Zhang, A. Debelle, L. Thomé, J.P. Crocombette, Z. Zihua, J. Jagielski, W.J. Weber, Damage processes in MgO irradiated with medium-energy heavy ions, Acta Mater. 88 (2015) 314–322.
[14] S. Moll, L. Thome, G. Sattonnay, A. Debelle, F. Garrido, L. Vincent, J. Jagielski, Multistep damage evolution process in cubic zirconia irradiated with MeV ions, J. Appl. Phys. 106 (2009), 073509.
[15] Y. Zhang, M.L. Crespillo, H. Xue, K. Jin, C.H. Chen, C.L. Fontana, J.T. Graham, W.J. Weber, New ion beam materials laboratory for materials modification and irradiation effects research, Nucl. Instrum. Methods Phys. Res. B 338 (2014) 19–30.
[16] K. Jin, H. Bei, Y. Zhang, Ion irradiation induced defect evolution in Ni and Ni-based FCC equiatomic binary alloys, J. Nucl. Mater. 471 (2016) 193–199.
[17] B.P. Uberuaga, R. Smith, A.R. Cleave, G. Henkelman, R.W. Grimes, A.F. Voter, K.E. Sickafus, Dynamical simulations of radiation damage and defect mobility in MgO, Phys. Rev. B 71 (2005) 104102.
[18] G. Sattonnay, F. Rullier-Albenque, O. Dimitrov, Determination of displacement threshold energies in pure Ti and in γ-TiAl alloys by electron irradiation, J. Nucl. Mater. 275 (1999) 63–73.
[19] D.K. Sood, G. Dearnaley, Radiation damage in copper single crystals, J. Vac. Sci. Technol. 12 (1975) 463–467.
[20] M.K. Agrawal, D.K. Sood, On the determination of the nature of defect clusters in irradiated metals by Rutherford backscattering, Nucl. Instrum. Methods 149 (1978) 425–427.
[21] J.A. Borders, J.M. Poate, Lattice-site location of ion-implanted impurities in copper and other fcc metals, Phys. Rev. B 13 (1976) 969–979.
[22] C. Lu, K. Jin, L.K. Beland, F. Zhang, T. Yang, L. Qiao, Y. Zhang, H. Bei, H.M. Christen, R.E. Stoller, L. Wang, Direct observation of defect range and

evolution in ion-irradiated single crystalline Ni and Ni binary alloys, Sci. Rep. 6 (2016) 19994.
[23] B.N. Singh, S.J. Zinkle, Defect accumulation in pure fcc metals in the transient regime: a review, J. Nucl. Mater. 206 (1993) 212–229.
[24] Y. Zhang, G.M. Stocks, K. Jin, C. Lu, H. Bei, B.C. Sales, L. Wang, L.K. Beland, R.E. Stoller, G.D. Samolyuk, M. Caro, A. Caro, W.J. Weber, Influence of chemical disorder on energy dissipation and defect evolution in concentrated solid solution alloys, Nat. Commun. 6 (2015) 8736.
[25] K. Jin, W. Guo, C. Lu, M.W. Ullah, Y. Zhang, W.J. Weber, L. Wang, J.D. Poplawsky, H. Bei, Effects of Fe concentration on the ion-irradiation induced defect evolution and hardening in Ni-Fe solid solution alloys, Acta Mater. 121 (2016) 365–373.
[26] E. Friedland, H.W. Alberts, M. Fletcher, Temperature dependence of damage ranges in some metals after argon implantation, Nucl. Instrum. Methods Phys. Res. B 45 (1990) 492–494.
[27] E. Friedland, H.W. Alberts, Radiation damage in nickel and iron after ion implantation, Nucl. Instrum. Methods Phys. Res. B 35 (1988) 244–246.
[28] A. Turos, L. Nowicki, A. Stonert, K. Pagowska, J. Jagielski, A. Muecklich, Monte Carlo simulations of ion channeling in crystals containing extended defects, Nucl. Instrum. Methods Phys. Res. B 268 (2010) 1718–1722.
[29] E. Wendler, O. Bilani, K. Gärtner, W. Wesch, M. Hayes, F.D. Auret, K. Lorenz, E. Alves, Radiation damage in ZnO ion implanted at 15K, Nucl. Instrum. Methods Phys. Res. B 267 (2009) 2708–2711.
[30] Y. Zhang, J. Lian, C.M. Wang, W. Jiang, R. Ewing, W.J. Weber, Ion-induced damage accumulation and electron-beam-enhanced recrystallization in $SrTiO_3$, Phys. Rev. B 72 (2005), 094112.